Mechanics of Materials 131 (2019) 113–120

Contents lists available at ScienceDirect

Mechanics of Materials

journal homepage: www.elsevier.com/locate/mechmat

Influence of surface energy and thermal effects on cavitation instabilities in metallic glasses

Huang X.[a], Ling Z.[b], Dai L.H.[b,c,*]

[a] Institute of Systems Engineering, China Academy of Engineering Physics, Mianyang, Sichuan 621999, China
[b] State Key Laboratory of Nonlinear Mechanics, Institute of Mechanics, Chinese Academy of Sciences, Beijing 100190, China
[c] School of Engineering Science, University of Chinese Academy of Sciences, Beijing 101408, China

ARTICLE INFO

Keywords:
Cavitation instabilities
Metallic glasses
Surface energy
Thermal effects

ABSTRACT

To reveal the void dominated fracture mechanism, cavitation instabilities in metallic glasses are studied through analytical and numerical approaches, with particular attention on surface energy and thermal effects. The critical pressure for unbounded growth of voids is determined, which increases apparently as surface energy is taken into account. A dimensionless number I_γ which is a ratio of the energy required to form new void surface and the energy dissipated by plastic deformation is proposed. It is found that the surface energy significantly impedes void growth at the early stage of void growth when I_γ is large. Besides, to address the thermal effects, another dimensionless number I_{th}, which reflects the competition of momentum diffusion and thermal diffusion, is presented. Results of numerical simulations show that the thermal effects first promote and finally impede the void growth at the late stage of void growth when $I_{th} \leq 1$. Further study on combined influence of inertia, surface energy and thermal effects reveals the factors which are dominant as the process develops.

1. Introduction

Metallic glasses are amorphous metastable solids fabricated by a fast quenching process. Different from traditional crystalline materials, they have atomic structures without translational orders, and lack structural defects such as vacancies, dislocations and grain boundaries. Due to this unique atomic structure, metallic glasses, on one hand, have excellent physical and mechanical properties including high strength, high hardness, good corrosion and wear resistance. On the other hand, plastic deformation in metallic glasses is very localized, and the fracture behavior usually is brittle, which impedes their wide application in many areas. Previous works have shown that shear bands are prone to be nucleated in metallic glasses under dynamic or even quasistatic loading: their fast propagation and interaction leads to macroscopic failure (Jiang and Dai, 2009). However, metallic glasses can also fail by cavitation instabilities (Huang et al., 2013,2016; Murali et al., 2011). This ductile fracture behavior has been confirmed by many experimental observations. Under quasistatic tensile loading, typical dimple patterns, nanoscale periodic corrugations and honeycomb structures were observed on the fracture surfaces of tested samples (Bouchaud et al., 2008), which indicated that the fracture occurs via cavitation instabilities. In spallation experiments, similar patterns such as void or dimple structures and equiaxed cellular patterns were found on the spalled surfaces of recovered samples, which implied that the spallation also takes place by void nucleation, growth and coalescence (Huang et al., 2011). Even in a shear instability process, cavities of different length scales can be found along the shear bands, which are a signature of a shear-band-to-crack transition (Liu and Maaß, 2018; Liu et al., 2017; Maaß et al., 2015). These works indicate that besides shear banding instabilities, cavitation instabilities are also the intrinsic response process under external stimuli in metallic glasses, which dominate the ductile fracture process at the microscopic scale.

Cavitation instabilities are the principal mechanism for ductile fracture in conventional crystalline materials, which have been intensively studied in the past few decades. It seems that Ball (1982) first recognized the existence of cavitation instabilities. By studying the response of a spherical cavity in a nonlinear elastic body under tension, a crucial concept of cavitation pressure was demonstrated to exist. The pressure is not only the critical condition for the bifurcation phenomenon from a defect-free solid to a solid containing a void, but also the pressure for continuous and unbounded growth of a pre-existing void (Horgan and Abeyaratne, 1986). The analysis was then extended to elastic-plastic materials with different initial void shapes and under axisymmetric remote stress states. It was found that the criterion for cavitation instabilities depends on the attainment of a critical value of the mean stress (Huang et al., 1991), and the initial void shape has little

* Corresponding author.
E-mail address: lhdai@lnm.imech.ac.cn (L.H. Dai).

https://doi.org/10.1016/j.mechmat.2019.01.019
Received 20 July 2018; Received in revised form 28 January 2019
Available online 29 January 2019

influence on cavitation pressure (Tvergaard and Hutchinson, 1993). Subsequent works from Wu et al. (2003) confirmed that the effects of thermal softening lower the threshold stress, while the effects of strain gradient greatly increase the threshold stress for cavitation instabilities. As the cavitation pressure is attained, it is important to address the factors which dominate the void growth process. Via investigation on void growth in a rigid-viscoplastic solid, Ortiz and Molinari (1992) indicated that the viscous effects are important at the early stage of void growth, while inertia tends to dominate the long-term response. Tong and Ravichandran (1995) examined the inertial effects on void growth in a viscoplastic material, they found that the inertia effects dominate for larger void size and higher loading rate. Recently, Wu et al. (2003) made a comprehensive study on dynamic void growth, their results showed that the effects of rate-hardening are to reduce the rate of void growth in the early stages of void growth, while the inertial effects first impede but finally promote the void growth. For the thermal effects, they are strongly affected by the initial void size. If the void is large enough, apparent thermal softening results in a higher growth rate.

Whereas much attention has been given to cavitation instabilities in conventional crystalline materials, the mechanism in metallic glasses remains relatively unclear. Bouchbinder et al. (2008) studied the dynamics of the boundaries of voids in metallic glasses, with the plasticity described by an athermal shear transformation zone theory. The existence of cavitation instabilities was predicted, and the threshold for unbounded growth was obtained. With the context of free volume theory, we use the single spherical void model to study cavitation instabilities in metallic glasses in our previous work (Huang et al., 2013). It is found that higher pressure sensitivity coefficient lowers the critical pressure for unbounded growth. The competition of inertial effects, loading rate effects and viscous effects dominates the dynamic void growth process. Moreover, Singh et al. (2013) investigated cavitation in metallic glasses with distributed weak zones. Their results showed that the critical pressure for cavitation instabilities is significantly decreased by the presence of weak zones, and does not reduce appreciably as the stress ratio decreases from unity. Although the above works shed lights into the nature of cavitation instabilities in metallic glasses, there are still some questions that have not been answered:

- Does surface energy have influence on void growth at the early stage in metallic glasses? Nanoscale periodic corrugations have been observed on the fracture surfaces, which implies that the growth process of voids in metallic glasses may occur at very small scales of 10° nm–10^{1} nm. The length scales are close to that of void nucleation (~1 nm), which is the creation of a void in defect-free solids with the size large enough to grow under applied stress field (Huang et al., 2011). As surface energy contributes much to the free energy barrier for void nucleation, it is expected that it may continue to play an important role at the early stage of the void growth process. However, these effects on void growth have drawn relatively little attention.
- How to address the thermal effects on void growth at the late stage in metallic glasses? Dimple structures and equiaxed cellular patterns larger than 10^{2} nm can be also found on the fracture surfaces of metallic glasses. At those length scales, temperature rise of matrix material surrounding the voids may become more and more apparent according to the results in conventional crystalline materials. As both the free volume softening and the thermal softening play important roles in viscous flow of the metallic glasses, it is worth to investigate the influence of thermal effects on void growth.

To this end, this paper studies cavitation instabilities in metallic glasses under remote tensile loading, with particular attention on surface energy and thermal effects. To take these effects into account, a virtual tensile pressure is assumed to be applied to the internal surface of the void, and a temperature evolution equation is added to the governing equations . The critical pressure for cavitation instabilities is determined theoretically, with the dependence on surface energy addressed. To examine the effects of surface energy on void growth, a dimensionless number which is a ratio of the energy required to form new void surface to the energy dissipated by plastic deformation surrounding the void is presented, and numerical simulations are carried out to quantify the effects. Besides, to address the thermal effects, another dimensionless number which reflects the competition of momentum diffusion and thermal diffusion is proposed. The influence of thermal effects on the evolution of free volume concentration and the change of material viscosity is studied. Finally, the combined influence of inertia, surface energy and thermal effects are investigated, and the roles that they play at different stages of void growth are discussed.

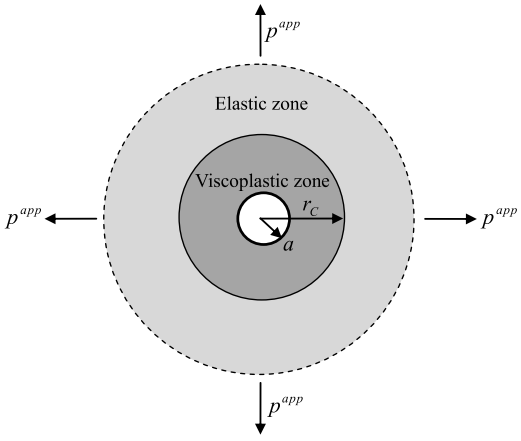

Fig. 1. Schematic diagram of a single void in an infinite body under remote hydrostatic tensile pressure. a is the void radius, p^{app} the applied tensile pressure, and r_C the elastic-viscoplastic boundary which divides the matrix material into two zones: the inner viscoplastic zone and the outer elastic zone.

2. General formulation

2.1. The basic model

We consider a spherical void of radius a in an infinite metallic glass under hydrostatic tensile loading. As shown in Fig. 1, the void grows as the remote hydrostatic tensile pressure is applied. As the material surrounding the void is homogenous and isotropic, both the void and the elastic-viscoplastic boundary are assumed to remain spherical throughout the growth process. Then, according to continuum mechanics, the equation of motion is written as:

$$\frac{d\sigma_r}{dr} + \frac{2}{r}(\sigma_r - \sigma_\theta) = \rho\ddot{r} \tag{1}$$

where σ_r and σ_θ are the principal stresses along the radial and tangential directions respectively. The metallic glass material surrounding the void is assumed to obey an elastic-viscoplastic constitutive law as:

$$\varepsilon_{ij} = \frac{s_{ij}}{2\mu} \text{ if } \tau + Qp \le \hat{\tau} - (C_1 T/T_g)^{1/2} \tag{2}$$

$$\dot{\varepsilon}_{ij} = \frac{\dot{s}_{ij}}{2\mu} + \frac{s_{ij}}{2\eta} \text{ if } \tau + Qp \ge \hat{\tau} - (C_1 T/T_g)^{1/2} \tag{3}$$

where ε_{ij} is the strain tensor deviator, s_{ij} the stress deviator, μ the shear modulus, and η the viscosity. To characterize the pressure sensitivity in plastic flow, the yield criterion of BMGs suggested by Sun et al. (2010) is used. In this criterion, $\tau = (\sigma_\theta - \sigma_r)/2$ is the maximum shear stress, $p = (\sigma_r + 2\sigma_\theta)/3$ is the hydrostatic pressure, Q is the pressure sensitivity coefficient and the term $\hat{\tau} - (C_1 T/T_g)^{1/2}$ represents the yield strength ($\hat{\tau}$ is the barrier shear resistance of a shear transformation zone-STZ, C_1 is a coefficient that reflects the dependence of strength on temperature, T

is the temperature, and T_g is the glass transition temperature).

The viscosity of metallic glasses is stress dependent, which is defined as (Steif, 1983):

$$\eta \equiv \frac{\tau_e}{\dot{\gamma}^p} = \frac{\tau_e}{2f\exp\left(-\frac{\Delta G^m}{k_B T}\right)\sinh\left(\frac{\tau^e \Omega}{2k_B T}\right)\exp\left(-\frac{1}{\xi}\right)} \tag{4}$$

where $\tau_e = \sqrt{J_2} = \sqrt{s_{ij}s_{ij}/2}$ is the effective shear stress, $\dot{\gamma}^p$ the plastic strain rate, f the frequency of atomic vibration (~Debye frequency), ΔG^m the activation energy, k_B the Boltzmann constant, Ω the atomic volume, and ξ the concentration of free volume ($\xi = v_f/\chi v^*$, here v_f, χ and v^* are, respectively, the free volume, a geometric factor and the effective hard-sphere size of an atom).

The free volume concentration is believed to be controlled by three processes: diffusion, annihilation and generation. Following Dai et al. (2005), the free volume obeys a diffusion equation:

$$\frac{\partial \xi}{\partial t} = D\nabla^2\xi + G(\xi, T, \tau, p) \tag{5}$$

$$G(\xi, T, \tau, p) = \frac{1}{\chi} f \exp[-\frac{1}{\xi}]\exp[-\frac{\Delta G_m}{k_B T}]\left\{\frac{2k_B T}{\xi v^* S}\left[\cosh(\frac{\tau_e \Omega}{2k_B T}) - 1\right] - \frac{1}{n_D}\right\} + \frac{\Omega \dot{p}}{\chi v^* \kappa} \tag{6}$$

where D is the diffusion coefficient of free volume concentration and $G(\xi, T, \tau, p)$ the net generation rate of free volume, S the effective shear modulus ($S = \frac{2(1+\nu)\mu}{3(1-\nu)}$ with ν being Poisson's ratio), n_D the number of diffusive jumps necessary to annihilate a free volume equal to v^*, and κ the bulk modulus. Here the generation of free volume is composed of two parts: the extra free volume created by a shear stress and the volume dilation of matrix material under negative pressure.

As the volume dilation is so small, the contribution to the displacement field can be neglected. Thus, we assume that the matrix material is incompressible, namely in terms of the radial and tangential strains,

$$\varepsilon_r + 2\varepsilon_\theta = 0 \tag{7}$$

2.2. Surface energy effects

To take the effects of surface energy into account, we assume that there is a virtual tensile pressure applied to the surface of the void. During the growth process, the work done by the virtual tensile pressure is equal to the energy required to form new void surface:

$$P_\gamma 4\pi a^2 da = \gamma[4\pi(a + da)^2 - 4\pi a^2] \tag{8}$$

where P_γ is the virtual tensile pressure, γ is the surface energy. According to previous works (Guan et al., 2013), the surface energy is curvature dependent at small radii which can be written as $\gamma = \gamma_\infty/(1 + 2\delta/a)$. Here γ_∞ is the surface energy of the flat surface and δ is a parameter called the Tolman length. Thus, we have

$$\sigma_r|_{r=a} = P_\gamma = 2\gamma_\infty/(a + 2\delta) \tag{9}$$

Then the effects of surface energy are converted to a boundary condition.

2.3. Thermal effects

To take the thermal effects into consideration, the equation of energy conservation is requested:

$$\rho c_p \frac{dT}{dt} = \lambda \frac{1}{r^2}\frac{\partial}{\partial r}(r^2\frac{\partial T}{\partial r}) + \beta_{TQ}\sigma_e \dot{\varepsilon}_e^p \tag{10}$$

where ρ is the density, c_p the specific heat at constant pressure, λ the thermal conductivity, β_{TQ} the Taylor–Quinney coefficient, and $\dot{\varepsilon}_e^p$ the effective plastic strain rate.

3. Analytical results of cavitation instabilities

To derive the criterion for unbounded growth of the void, we consider the quasistatic case. As there is enough time for the heat to be conducted away in this case, the thermal effects can be neglected, and we focus on the effects of surface energy. In spherical coordinates, the equation of equilibrium is

$$\frac{d\sigma_r}{dr} + \frac{2}{r}(\sigma_r - \sigma_\theta) = 0 \tag{11}$$

with the boundary conditions

$$\sigma_r|_{r=a} = 2\gamma_\infty/(a + 2\delta) \text{ and } \sigma_r|_{r=\infty} = p^{app} \tag{12}$$

If the applied loading is sufficiently high, the matrix material surrounding the void is divided into two zones by the elastic-viscoplastic boundary at $r = r_C$. In the elastic zone $r \geq r_C$, the stress components and radial displacement are

$$\sigma_r = p^{app} - \frac{4}{3}[\hat{\tau} - (C_1 T/T_g)^{1/2} - Qp^{app}]\frac{r_C^3}{r^3} \tag{13}$$

$$\sigma_\theta = p^{app} + \frac{2}{3}[\hat{\tau} - (C_1 T/T_g)^{1/2} - Qp^{app}]\frac{r_C^3}{r^3} \tag{14}$$

$$u_r = \frac{1}{3\mu}[\hat{\tau} - (C_1 T/T_g)^{1/2} - Qp^{app}]\frac{r_C^3}{r^2} \tag{15}$$

In the viscoplastic zone $a \leq r \leq r_C$, the equilibrium equation becomes

$$\frac{d\sigma_r}{dr} = \frac{12}{3 + 4Q}\frac{-Q\sigma_r + \hat{\tau} - (C_1 T/T_g)^{1/2}}{r} \tag{16}$$

Using the boundary condition at $r = a$ and the contininuity of radial stress σ_r across the elastic-viscoplastic boundary, we can obtain

$$p^{app} = \frac{\hat{\tau} - (C_1 T/T_g)^{1/2}}{Q} - \frac{3}{Q(3 + 4Q)}[\hat{\tau} - (C_1 T/T_g)^{1/2} - 2\gamma_\infty Q/(a + 2\delta)]\frac{a^{12Q/(3+4Q)}}{r_C^{12Q/(3+4Q)}} \tag{17}$$

Following Hill's analysis (Hill, 1950) and our previous work (Huang et al., 2013), if the elastic-viscoplastic boundary r_C is taken as the scale of "time", the velocity v of a particle means that the particle is displaced by an amount $vdr_C$when the elastic–viscoplastic boundary moves outwards a further distance dr_C. Thus, we have

$$v = \frac{\partial u_r/\partial r_C}{1 - (\partial u_r/\partial r)} \tag{18}$$

and the equation of incompressibility is rewritten as

$$\frac{\partial v}{\partial r} + \frac{2v}{r} = 0 \tag{19}$$

On the elastic–viscoplastic boundary, v can be calculated from Eqs. (15) and (18), that is

$$v|_{r=r_C} = \frac{\hat{\tau} - (C_1 T/T_g)^{1/2} - Qp^{app}}{\mu} \tag{20}$$

Solving Eq. (19) with the boundary condition Eq. (20), leads to

$$v = \frac{[\hat{\tau} - Qp^{app} - (C_1 T/T_g)^{1/2}]r_C^2}{\mu r^2} \tag{21}$$

On the void surface, $v = da/dr_C$, the relation between a and r_C is

$$\frac{da}{dr_C} = \frac{[\hat{\tau} - Qp^{app} - (C_1 T/T_g)^{1/2}]r_C^2}{\mu a^2} \tag{22}$$

Using the initial condition when $r_C = a$ yields

Table 1
Material parameters for Vitreloy 1.

Parameters	Notation	Value
Shear modulus	μ	35.3 GPa
Density	ρ	6125 kg m^{-3}
Free-volume diffusivity	D	$\sim 10-16$ m^{2}s^{-1}
Average atomic volume	Ω	20 Å^3
Activation energy	ΔG^m	0.2–0.5 eV
Frequency of atomic vibration	f	~ 1013 s^{-1}
Boltzmann constant	k_B	13.8×10^{-24} J/K
Pressure sensitivity coefficient	Q	0.158
Glass transition temperature	T_g	638 K
Geometric factor	χ	0.105
Effective hard-sphere size of atom	v^*	20 Å^3
Bulk modulus	K	112.7 GPa
Effective shear modulus	S	50.0 GPa
Jump number for annihilation	n_D	6
Shear strength at ambient temperature	$\hat{\tau} - (C_1 T/T_g)^{1/2}$	823.3 MPa
Surface energy	γ	0.83 J m^{-2}
Tolman length	δ	1.15 Å
Specific heat at constant pressure	c_p	~ 400 J kg^{-1}K^{-1}
Thermal conductivity	λ	20 W m^{-1}K^{-1}
Taylor–Quinney coefficient	β_{TQ}	0.9

$$p^{app}|_{r_C=a} = \frac{4[\hat{\tau} - (C_1 T/T_g)^{1/2}] + 6\gamma_\infty/(a+2\delta)}{3+4Q} \tag{23}$$

$$u_r|_{r_C=a} = a - A = \frac{3[\hat{\tau} - (C_1 T/T_g)^{1/2}]a - 6Q\gamma_\infty a/(a+2\delta)}{(3+4Q)\mu} \tag{24}$$

According to the results of previous works (Guan et al., 2013; Huang et al., 2011), the critical radius of void nucleation ($\sim$1 nm) can be used to estimate the initial void radius A, and a lies between 1 nm to about 10 μm. The Tolman length is about 1.15 Å for a Zr-based metallic glass (Guan et al., 2013). As a rough estimate, $a/(a+2\delta) \approx 1$, we have

$$a|_{r_C=a} = \frac{A(3+4Q)\mu - 6Q\gamma_\infty}{(3+4Q)\mu - 3[\hat{\tau} - (C_1 T/T_g)^{1/2}]} \tag{25}$$

To simplify Eq. (25), we choose Vitreloy 1 as the model material, the values of material parameters can be found in Table 1 (Huang et al., 2013). Then, we can estimate the order of each term on the right hand side. As $A/(3+4Q)\mu \gg 6Q\gamma_\infty$ and $(3+4Q)\mu \gg 3[\hat{\tau} - (C_1 T/T_g)^{1/2}]$, Eq. (25) can be rewritten as

$$a|_{r_C=a} = A \tag{26}$$

Solving Eq. (22) with the initial condition, there results

$$a^3 = \frac{[\hat{\tau} - (C_1 T/T_g)^{1/2} - Qp^{app}]r_C^3}{\mu} + \left[1 - \frac{3[\hat{\tau} - (C_1 T/T_g)^{1/2}] - 6Q\gamma_\infty/(A+2\delta)}{(3+4Q)\mu}\right]A^3 \tag{27}$$

If cavitation instabilities occur, the relative void size goes to infinity, i.e., $a/A \to \infty$ or $A \to 0$. Then, in terms of the current void size, the position of the elastic–viscoplastic boundary is

$$\frac{r_C}{a} = \left[\frac{\mu}{\hat{\tau} - Qp^{app} - (C_1 T/T_g)^{1/2}}\right]^{1/3} \tag{28}$$

Thus, with Eqs. (17) and (27), we have

$$p^{app} = \frac{\hat{\tau} - (C_1 T/T_g)^{1/2}}{Q} - \frac{[3\hat{\tau} - 3(C_1 T/T_g)^{1/2} - 6Q\gamma_\infty/(a+2\delta)]^{(3+4Q)/3}}{Q(3+4Q)^{(3+4Q)/3}\mu^{4Q/3}} \tag{29}$$

It is obvious that p^{app} decreases with the increasing of the current void radius a. The threshold for cavitation instabilities is determined by the maximum value of p^{app} when $a = A$. Using the typical material parameters and the critical radius of void nucleation $\sim$1 nm for a, the change of cavitation pressure as a function of surface energy is shown in Fig. 2. Higher surface energy is corresponding to higher critical pressure for cavitation instabilities. For Vitreloy 1, the cavitation pressure increases from about 3.3 GPa–4.0 GPa when the surface energy effects are considered. Thus, it is expected that cavitation instabilities are prone to occur at the sites with lower local surface energy in metallic glasses which is in accordance with the results of molecular dynamics simulations (Guan et al., 2013).

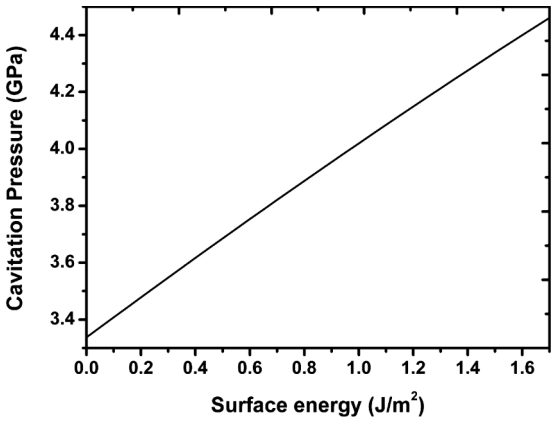

Fig. 2. Cavitation pressure as a function of surface energy.

4. Numerical simulations of void growth

4.1. Details of the numerical simulation

To reveal the influence of surface energy and thermal effects, growth of voids is studied via numerical simulations. The full set of Eqs. (1)–(10) are solved with the finite difference method (FDM) for dynamic void growth cases, while Eqs. (2)–(11) are solved for quasistatic cases. Following Bouchbinder et al. (2008), a time-dependent coordinate transformation is applied to avoid dealing with an infinite time-dependent domain:

$$x = \frac{a(t)}{r} \tag{30}$$

Thus, integration of equations in the time-independent finite domain $x \in (0, 1)$ is allowed. This domain is uniformly discretized with 101 nodes, while the time domain is discretized with sufficiently small time steps so that the numerical error is acceptable. Each result is checked to make sure that it will not change if the spatial mesh is refined.

For comparison with our previous work, a similar form of hydrostatic tensile loading applied on the outer boundary ($x = 0$) is adopted as shown in Fig. 3. There are two stages in the loading history: (1) the rise stage in which the applied loading linearly increases to a desired amplitude p_S after a rise time t_a, and (2) the steady stage in which the loading amplitude is held constant for a time t_S. A typical metallic glass Vitreloy 1 is chosen as a model material with material parameters listed in Table 1.

To find the critical pressure for cavitation instability via the numerical method, void growth with variation of loading amplitudes is examined. Consider three cases with the loading amplitude p_S ranging from 2 GPa to 4 GPa. In each case, the inertial effects and thermal effects which usually play important roles at the late stage of void growth are not considered, and other parameters remain the same: the initial void size A is 10 nm, the ambient temperature $T_i = 300$ K, initial free volume concentration $\xi_i = 0.05$, the surface energy $\gamma_\infty = 0.83$ J/cm^2, the Tolman length $\delta = 1.15$ Å, and the loading rate $q = 0.1$ GPa/ns. The numerical results are shown in Fig. 4. It is obvious that a critical pressure p_{cr}^{app} for unbounded growth exists between 3 GPa and 4 GPa,

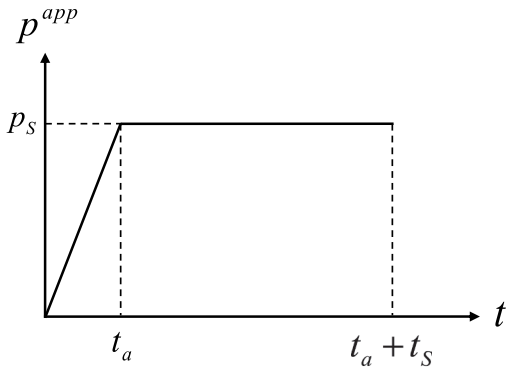

Fig. 3. Loading history of applied tensile pressure. The loading history contains two stages: the rise stage in which the applied pressure increases linearly until the desired loading p_S is achieved after a rise time t_a, and the steady stage in which the loading is held constant at p_S during the hold time t_S.

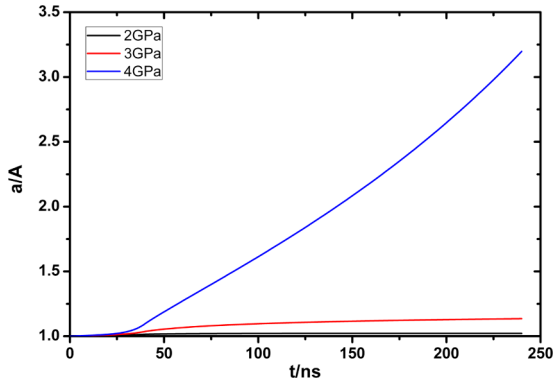

Fig. 4. Numerical results on void growth under different loading amplitudes of 2 GPa, 3 GPa and 4 GPa.

which is consistent with the analytic model.

4.2. Influence of surface energy on void growth

In this section, we examine the influence of surface energy on early growth of voids. As previous works (Huang et al., 2013; Wu et al., 2003) had shown that thermal effects and inertial effects play more important roles at the late stage of void growth when the void radii are large enough, here both thermal effects and inertial effects are not considered.

As the effects of surface energy are determined by the magnitude of the virtual tensile pressure, we begin by scaling the Eq. (9) first. Choosing the initial void radius A as the scale of space and the loading amplitude p_S as the scale of stress, the scaled equation is

$$\tilde{\sigma}_r\Big|_{r=a} = \tilde{P}_\gamma = \frac{2\gamma_\infty}{(\tilde{a} + \delta/A)AP_S} \tag{31}$$

where $\tilde{\sigma}_r = \sigma_r/P_S$, $\tilde{P}_\gamma = P_\gamma/P_S$ and $\tilde{a} = a/A$. In Eq. (31), $\tilde{a}$ is typically of order unity at the very early stage of void growth, and δ/A is less than 1, then the order of $\tilde{P}_\gamma$ is determined by the following dimensionless factor:

$$I_\gamma = \frac{2\gamma_\infty}{AP_S} \tag{32}$$

In fact, during void growth process, the radius of the plastic region is proportional to the void radius, which is indicated by Eq. (28). Thus, AP_S is proportional to the energy (per unit area) dissipated by plastic deformation under applied loading in the matrix material surrounding the void. As $2\gamma_\infty$ represents the energy (per unit area) required to form new void surface, the dimensionless number I_γ is indeed an energy ratio

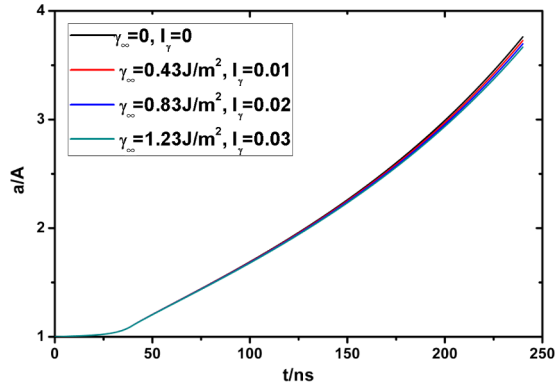

(a) A = 100 nm

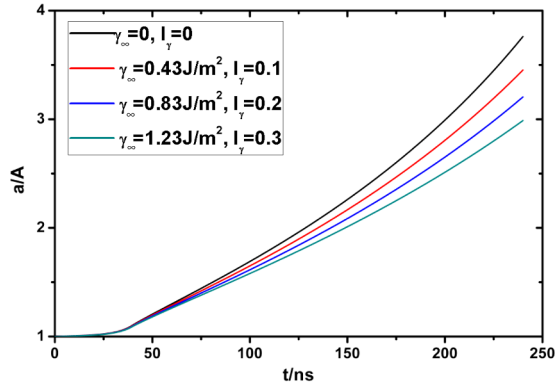

(b) A = 10 nm

Fig. 5. Effects of surface energy on void growth with two initial void radii A.

which reflects the competition of surface energy effects and plastic deformation under applied loading. The larger I_γ becomes, the more influence on void growth the surface energy effects have.

To further characterize the surface energy effects, we consider the initial void radius A ranging from 10 nm to 100 nm, and the surface energy γ_∞ varying from 0 to 1.23 J/cm^2. As there are nanoscale structural heterogeneities in MGs (Liu et al., 2011; Murali et al., 2011), here void growth with much smaller void radius is not discussed to guarantee the continuum model. In each case, the loading amplitude is 4 GPa, the loading rate $q = 0.1$ GPa/ns, the ambient temperature $T_i = 300$ K, the Tolman length $\delta = 1.15$ Å, and the initial free volume concentration $\xi_i = 0.05$. Here the thermal softening and inertial effects are not taken into consideration, all cases are quasistatic and in athermal condition.

The results of numerical simulations on void growth with different void radii and different surface energies are presented in Fig. 5. As shown in Fig. 5(a), for voids with the initial radius $A = 100$ nm, the growth rate of voids is nearly the same, which implies that the effects of surface energy can be neglected. But for voids with the initial radius $A = 10$ nm as shown in Fig. 5(b), the growth rate of voids decrease obviously as the value of surface energy becomes larger. It is expected that surface energy effects will impede the void growth significantly as the void radius is smaller. These results also imply that void growth is dependent on the specific alloy system, as the growth rate is influenced by surface energy.

The numerical results are in good agreement with our expectations from the scaling analysis presented in this section. When the initial void radius is 1 nm, the dimensionless number I_γ is of order unity. This means that the virtual tensile pressure applied to the inner surface of voids is comparable with the external tensile loading. As the energy required to form new void surface is comparable with the energy dissipated by plastic deformation under applied loading, the surface energy effects will significantly impede the void growth process. But as

the initial void radii increase to 10 nm and 100 nm, the dimensionless number I_γ decreases by 1–2 orders. Compared with plastic deformation of matrix material surrounding the voids, the energy required to form new void surface is much smaller. It is expected that the growth rate of voids approaches the case with the surface energy $\gamma_\infty = 0$ gradually.

4.3. Influence of thermal effects on void growth

In this section, we examine the thermal effects on void growth. Both thermal effects and inertial effects play important roles at the late stage of void growth. For simplification, the influence of inertial effects is excluded, and the equation of static equilibrium (Eq. (11)) is used in our numerical simulations.

To address the thermal effects, we begin scaling the temperature evolution equation first. Choosing the initial void radius A, the loading amplitude p_S, and the relaxation time $t_r = \eta/\mu$ as the scales of space, stress and time, the scaled equation is

$$\frac{d\tilde{\theta}}{d\tilde{t}} = \frac{\lambda t_r}{\rho c_p A^2}\frac{1}{\tilde{r}^2}\frac{\partial}{\partial \tilde{r}}\left(\tilde{r}^2\frac{\partial \tilde{\theta}}{\partial \tilde{r}}\right) + \beta_{TQ}\tilde{\sigma}_e\dot{\tilde{\varepsilon}}^p \tag{33}$$

where $\tilde{\theta} = \rho c_p\theta/P_S$, $\tilde{t} = t/t_r$, $\tilde{r} = r/A$, and $\tilde{\sigma}_e = \sigma_e/P_S$. As shown in Eq. (33), the temperature of the matrix material is determined by the heat conduction and the heat generated by plastic deformation. For void growth process, plastic deformation occurs in very localized region near the void surface. Thus, plastic deformation induces the heat to accumulate in the matrix material near the void surface, but the heat conduction moves the heat from inner hot region towards outer cooler region. The rates of plastic deformation and heat conduction determine which factor dominates the temperature evolution process. To characterize the competition of heat diffusion and generation by plastic deformation, we propose a dimensionless number as follows:

$$I_{th} = \frac{\lambda t_r}{\rho c_p A^2} = \frac{t_r}{t_d} \tag{34}$$

I_{th} consists of two characteristic time scales: (1) the relaxation time scale t_r, which is the characteristic time for viscous flow, and can also be interpreted as the time scale for momentum diffusion, in which process elastic strain energy is released to drive the viscoplastic deformation around the void, leading to growth of the void and generation of heat; (2) the thermal diffusion time scale $t_d = A^2/\kappa$ ($\kappa = \lambda/\rho c$ is thermal diffusion coefficient), which can be interpreted as the time scale for heat moving away from the viscoplastic region near the void surface. If I_{th} becomes larger, or the relaxation time scale t_r becomes larger than the thermal diffusion time scale t_d, thermal diffusion will become faster than momentum diffusion, which implies that heat is conducted away faster than its generation. Thus, temperature rise of the matrix material around the void hardly occurs, and thermal effects have fewer influence on void growth.

Besides the material parameters of the matrix material, the value of I_{th} depends on the initial void radius A. To further characterize the thermal effects, numerical simulations are carried out. We consider 4 cases with different initial void radii which are 10 nm, 100 nm, 1 μm and 10 μm respectively, and an athermal case and an adiabatic case are presented for comparison. In each case, the loading amplitude is 4 GPa, the loading rate $q = 0.1$ GPa/ns, the ambient temperature $T_i = 300$ K, and the initial free volume concentration $\xi_i = 0.05$. Here the inertial effects and the surface energy effects are not taken into consideration, all cases are in quasistatic condition with $\gamma_\infty = 0\ \mathrm{J/m^2}$.

Fig. 6 illustrates the numerical results of void growth process with different initial void radii. For the case with the initial void radius $A = 10$ nm, the growth rate of the void is the lowest. There is no apparent difference from the athermal case. As the initial void radius increases to 100 nm, the growth rate of voids begins to increase. However, as the initial void radius reaches 1 μm and larger, the growth rate slows down apparently. For the case with the initial void radius of

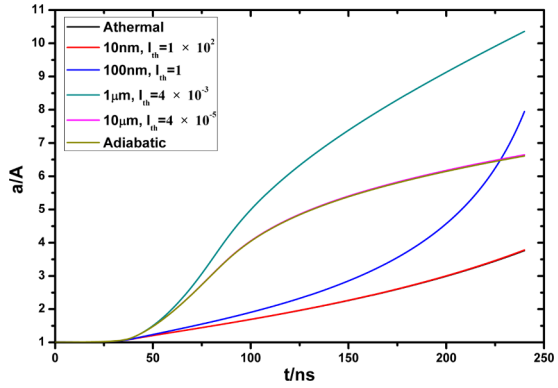

Fig. 6. Effects of thermal softening on void growth with 4 initial void radii. Six cases are considered: (a) an athermal case; (b) $A = 10$ nm; (c) $A = 100$ nm; (d) $A = 1$ μm; (e) $A = 10$ μm; (f) an adiabatic case.

10 μm, the result approaches to the adiabatic case. In fact, these results are somewhat out of our expectation, especially the decrease of growth rate as the initial void radii becomes 1 μm and larger. In conventional crystalline materials, thermal softening which leads to decrease of material viscosity should be very apparent in the cases approaching the adiabatic condition. It is believed that the void will grow faster when the temperature rises higher. However, our results show that extreme temperature rise will lead to an opposite tendency.

To understand the phenomenon, we examined the evolution of material viscosity on the void surface during the void growth process as illustrated in Fig. 7. As other factors such as the inertial effects, the loading rate effects and the surface energy effects are not taken into consideration, the growth of voids is dominated by the viscous effects. For the case with the initial void radius of 10 nm, the material viscosity first drops to about 57 Pa·s at the rise stage of loading history, and then keeps nearly constant at the steady stage. As the initial void radius increases to 100 nm, the variation of viscosity during the growth process is similar, but value of viscosity is lower, which leads to a faster growth of the void. However, as the void radii become 1 μm or larger, the viscosity first drops to a much lower value, and then increases significantly at the late stage of the loading history (after ~ 80 ns). As the viscosity is much higher, the void growth rate decreases significantly.

To address the role that thermal effects play during the void growth process, we further examined the dimensionless number I_{th}. For the cases with the initial void radii of 10 nm, 100 nm, 1 μm, 10 μm, the minimum values of viscosity of the matrix material are 57 Pa·s, 48 Pa·s, 16 Pa·s and 17 Pa·s. With other material parameters listed in Table 1, we can calculate the corresponding value of I_{th}, which is about

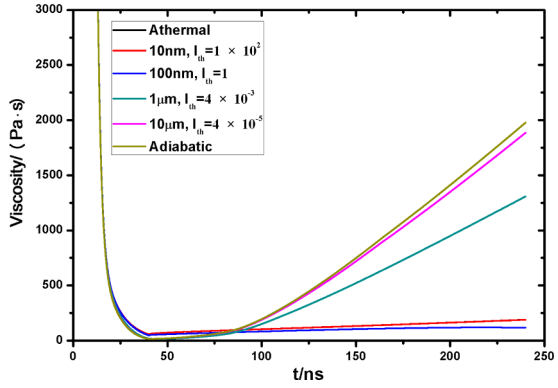

Fig. 7. Evolution of viscosity on the void surface during the growth process. The cases plotted are: (a) an athermal case; (b) $A = 10$ nm; (c) $A = 100$ nm; (d) $A = 1$ μm; (e) $A = 10$ μm; (f) an adiabatic case.

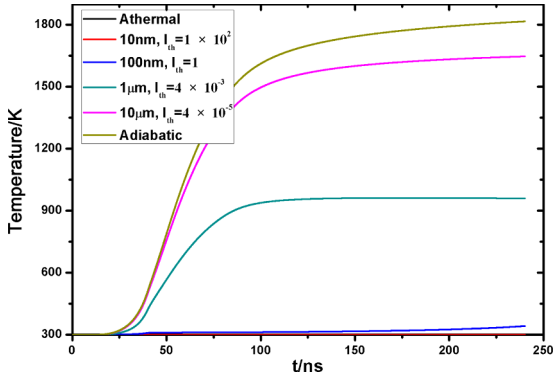

Fig. 8. Evolution of temperature on the void surface during the growth process. The cases plotted are: (a) an athermal case; (b) $A = 10$ nm; (c) $A = 100$ nm; (d) $A = 1$ μm; (e) $A = 10$ μm; (f) an adiabatic case.

1×10^2, 1, 4×10^{-3}, 4×10^{-5}, respectively. As the initial void radius increases, I_{th} decreases by several orders. If I_{th} is small, it means the release rate of elastic energy is so fast that there is not enough time for heat to be conducted away from the inner hot region. The temperature rise of the matrix material is significant. Fig. 8 shows the history of material temperature on the void surface during the growth process. For the case $I_{th} = 1 \times 10^2$, the temperature of the matrix material on the void surface keeps constant at the ambient temperature of 300 K. As I_{th} increases to 1, a slight increase of temperature can be observed. For the cases with $I_{th} = 4 \times 10^{-3}$ and smaller, the temperature rise is more than 600 K, gradually approaching the adiabatic case. It seems that there is a transition boundary lying at $I_{th} = 1$ (or $A = 100$ nm), where the rate of momentum diffusion is compatible with the rate of thermal diffusion. When $I_{th} >> 1$ (or $A < 100$ nm), thermal diffusion is much faster than momentum diffusion. It is expected that the temperature rise of the material is not significant. But when $I_{th} \leq 1$, heat can accumulate at the matrix material surrounding the voids, and thermal effects begin to be effective during the void growth process. The phenomenon of temperature rise during the fracture process in metallic glasses has been observed in some recent works (Das et al., 2018).

In metallic glasses, temperature rise can not only induce softening of the material, but also the annihilation of free volume. The viscosity depends on both the material temperature and the free volume concentration. Fig. 9 presents the evolution of free volume concentration on the void surface during the growth process. At the early stage of the loading history (during 0–20 ns), the total amount of free volume increases linearly with the increasing applied loading. After yielding of matrix material on the void surface, the change of free volume concentration exhibits some different features. For the cases with $I_{th} >> 1$, as the matrix material keeps at ambient temperature, the annihilation

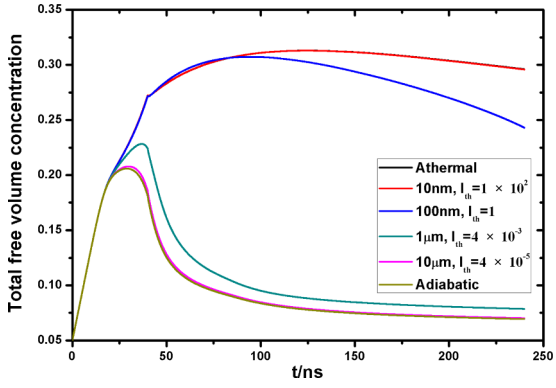

Fig. 9. Evolution of free volume concentration on the void surface during the growth process. The cases plotted are: (a) an athermal case; (b) $A = 10$ nm; (c) $A = 100$ nm; (d) $A = 1$ μm; (e) $A = 10$ μm; (f) an adiabatic case.

of free volume is very slow. Thus, the total amount of free volume continues to increase at the rest of the rise stage of loading history and then nearly keeps constant at the steady stage. Here, the decrease of viscosity is just determined by free volume softening. When the thermal effects begin to work ($I_{th} = 1$), a slight increase of temperature, on one hand, facilitates the faster creation of free volume during 40–80 ns. On the other hand, the rise of temperature, in favor of the annihilation of free volume, results in a slight decrease of the free volume concentration at the late stage of loading history (after 80 ns). The coupling of free volume softening and thermal softening leads to a lower viscosity and a faster void growth rate. But for the cases with $I_{th} << 1$, as the material temperature significantly increases, the annihilation of free volume is very fast. This results in a drastic decrease of the free volume concentration, and in a significant increase of material viscosity which lowers the void growth rate. In metallic glasses, the diameters of dimples and voids observed in quasistatic and dynamic tensile tests are always less than 10 μm (Bouchaud et al., 2008; Huang et al., 2011). It is obvious that void growth is impeded as the void size becomes large. The decrease of void growth rates is attributed either to inertial effects or to thermal effects.

4.4. Combined influence of inertia, surface energy and thermal effects on void growth

The inertial effects have not been accounted for in the results so far. Here, we continue to examine the combined influence of inertia, surface energy and thermal effects on void growth. According to our previous work (Huang et al., 2013), if the loading effects are not considered, the growth of voids is controlled by a dimensionless inertial number:

$$I_{inertia} = \frac{t_{inertia}}{t_r} \tag{35}$$

where $t_{inertia} = A/\sqrt{p_S/\rho}$ is the inertial time scale, which is a characteristic time of outward flux of matter, $t_r = \eta/\mu$ is the relaxation time scale, which is a characteristic time of viscous flow. As larger initial void radii lead to larger inertial number $I_{inertia}$, the inertial effects are expected to become important at the late stage of void growth.

Fig. 10 shows the void growth with combined influence of inertia, surface energy and thermal effects (plotted by solid lines). The results of quasistatic cases in which the inertia effects are excluded are also provided for comparison. In each case, the loading amplitude is 4 GPa, the loading rate $q = 0.1$ GPa/ns, the ambient temperature $T_i = 300$ K, the surface energy $\gamma_\infty = 0.83$ J/m^2, the Tolman length $\delta = 1.15$ Å, and the initial free volume concentration $\xi_i = 0.05$. For the cases with the initial void radii $A < 1$ μm, the influence of inertial effects can be neglected. Conversely for initial void radii $A \geq 1$ μm, the void growth is

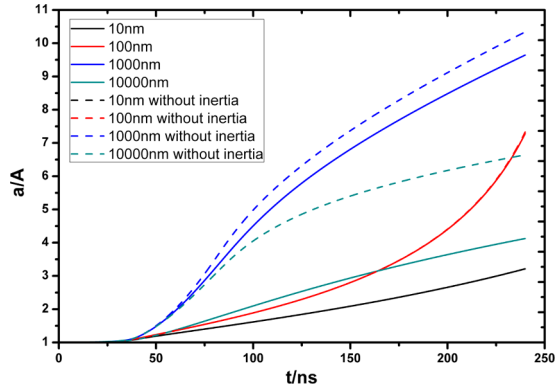

Fig. 10. Combined influence of inertia, surface energy and thermal effects on void growth with different radii. The cases plotted with solid lines are dynamic: (a) $A = 10$ nm; (b) $A = 100$ nm; (c) $A = 1$ μm; (d) $A = 10$ μm. The cases plotted with dash lines are quasistatic for comparison: (e) $A = 10$ nm; (f) $A = 100$ nm; (g) $A = 1$ μm; (h) $A = 10$ μm.

apparently impeded by inertial effects.

Comparing Figs. 5, 6 and 10, it is obvious that the surface energy effects impede void growth at the early stage when the void radius is smaller than 100 nm, while the thermal effects and inertial effects can be neglected. As the void grows larger than 100 nm (smaller than 1 μm), the surface energy effects are not important, but the thermal effects should be taken into consideration. Small amount of temperature rise leads to apparent thermal softening of the matrix material which gradually promotes the void growth. When it comes to the late stage when the void radii is larger than 1 μm, both thermal effects and inertial effects become dominant. Different from the inertial effects which merely impede the void growth, the thermal effects are more intricate. As heat can easily accumulate in the matrix material, temperature rise is very high at this stage. It not only contributes to thermal softening of the material, but also helps annihilation of free volume. Thus, the thermal effects first promote then impede void growth.

5. Conclusion

To address the void-dominant fracture process in metallic glasses, a theoretical description for void growth under remote tensile loading is presented, with particular attention on the influence of the surface energy and thermal effects. A brief conclusion is listed as follows:

- The effects of surface energy on void growth can be taken into account via a virtual tensile pressure applied to internal surface of the void, by which the work done is equal to the energy required to form new void surface. As the critical radius of void nucleation in metallic glasses is of order of 1 nm, the critical pressure for cavitation instabilities is apparently increased when surface energy is included.
- A dimensionless number $I_\gamma = 2\gamma_\infty/(AP_S)$, which is a ratio of the energy required to form new void surface and the energy dissipated by plastic deformation under applied loading, is proposed to characterize the effects of surface energy on void growth. The larger I_γ, the more dominant role the surface energy will play.
- The results of numerical simulations shows that the effects of surface energy have much influence on void growth when the void radius is small. For the void radius less than 10 nm ($I_\gamma \sim 1$), surface energy can significantly impede the void growth. As the void radii are larger than 100 nm ($I_\gamma << 1$), the influence of surface energy can be neglected.
- To characterize the thermal effects, another dimensionless number I_{th}, which consists of the relaxation time scale t_r and the thermal diffusion time scale t_d, is proposed. It reflects the competition between momentum diffusion and thermal diffusion. I_{th} is smaller, the thermal effects will play a more dominant role.
- The results of numerical simulations show that the influence of thermal effects is significant when the void radius is large. For the void radii larger than 100 nm ($I_{th} \leq 1$), thermal effects first promote, and finally impede the void growth.
- Further study on free volume dynamics indicates that, as the temperature rise is small, the coupling of free volume softening and thermal softening will significantly lower the material viscosity. But when the temperature rise is large, the free volume concentration drastically decreases due to the fast annihilation of free volume, and then leads to the significant increase of material viscosity and lower rate of void growth.
- When the inertia, surface energy and thermal effects are all taken into consideration, it is revealed that the surface energy effects are important at the early stage when the void radius is smaller than 100 nm, thermal effects begin to work when the void radius is larger than 100 nm, and both inertial effects and thermal effects are dominant factors on void growth when void radius is larger than 1 μm.

Acknowledgments

The work is financially supported by the National Key Research and Development Program of China (no. 2017YFB0702003), the NSFC (grant nos. 11772313, 11402245, 11272328, 11790292, 11472287), the Strategic Priority Research Program of the Chinese Academy of Sciences (grant nos. XDB22040302 and XDB22040303), the Key Research Program of Frontier Sciences of the Chinese Academy of Sciences (grant no. QYZDJSSW-JSC011), and the key subject “Computational Solid Mechanics” of the China Academy of Engineering Physics.

References

Ball, J.M., 1982. Discontinuous equilibrium solutions and cavitation in nonlinear elasticity. Philos. Trans. R. Soc. Lond. A 306, 557–611.
Bouchaud, E., Boivin, D., Pouchou, J.L., Bonamy, D., Poon, B., Ravichandran, G., 2008. Fracture through cavitation in a metallic glass. Europhys. Lett. 83, 66006.
Bouchbinder, E., Lo, T.S., Procaccia, I., 2008. Dynamic failure in amorphous solids via a cavitation instability. Phys. Rev. E 77, 025101.
Dai, L.H., Yan, M., Liu, L.F., Bai, Y.L., 2005. Adiabatic shear banding instability in bulk metallic glasses. Appl. Phys. Lett. 87, 141916.
Das, A., Kagebein, P., Küchemann, S., Maaß, R., 2018. Temperature rise from fracture in a Zr-based metallic glass. Appl. Phys. Lett. 112, 261905.
Guan, P., Lu, S., Spector, M.J.B., Valavala, P.K., Falk, M.L., 2013. Cavitation in amorphous solids. Phys. Rev. Lett. 110, 185502.
Hill, R., 1950. The Mathematical Theory of Plasticity. Oxford University Press, Oxford.
Horgan, C.O., Abeyaratne, R., 1986. A bifurcation problem for a compressible nonlinearly elastic medium: growth of a micro-void. J. Elast. 16, 189–200.
Huang, X., Ling, Z., Dai, L.H., 2013. Cavitation instabilities in bulk metallic glasses. Int. J. Solids Struct. 50, 1364–1372.
Huang, X., Ling, Z., Wang, Y.J., Dai, L.H., 2016. Intrinsic structural defects on medium range in metallic glasses. Intermetallics 75, 36–41.
Huang, X., Ling, Z., Zhang, H.S., Ma, J., Dai, L.H., 2011. How does spallation microdamage nucleate in bulk amorphous alloys under shock loading? J. Appl. Phys. 110, 103519.
Huang, Y., Hutchinson, J.W., Tvergaard, V., 1991. Cavitation instabilities in elastic-plastic solids. J. Mech. Phys. Solids 39, 223–241.
Jiang, M.Q., Dai, L.H., 2009. On the origin of shear banding instability in metallic glasses. J. Mech. Phys. Solids 57, 1267–1292.
Liu, C., Maaß, R., 2018. Elastic fluctuations and structural heterogeneities in metallic glasses. Adv. Funct. Mater. 28, 1800388.
Liu, C., Roddatis, V., Kenesei, P., Maaß, R., 2017. Shear-band thickness and shear-band cavities in a Zr-based metallic glass. Acta Mater. 140, 206–216.
Liu, Y.H., Wang, D., Nakajima, K., Zhang, W., Hirata, A., Nishi, T., Inoue, A., Chen, M.W., 2011. Characterization of nanoscale mechanical heterogeneity in a metallic glass by dynamic force microscopy. Phys. Rev. Lett. 106, 125504.
Maaß, R., Birckigt, P., Borchers, C., Samwer, K., Volkert, C.A., 2015. Long range stress fields and cavitation along a shear band in a metallic glass: the local origin of fracture. Acta Mater. 98, 94–102.
Murali, P., Guo, T., Zhang, Y., Narasimhan, R., Li, Y., Gao, H., 2011. Atomic scale fluctuations govern brittle fracture and cavitation behavior in metallic glasses. Phys. Rev. Lett. 107, 215501.
Ortiz, M., Molinari, A., 1992. Effect of strain-hardening and rate sensitivity on the dynamic growth of a void in a plastic material. J. Appl. Mech. Trans. ASME 59, 48–53.
Singh, I., Guo, T.F., Murali, P., Narasimhan, R., Zhang, Y.W., Gao, H.J., 2013. Cavitation in materials with distributed weak zones: implications on the origin of brittle fracture in metallic glasses. J. Mech. Phys. Solids 61, 1047–1064.
Steif, P.S., 1983. Ductile versus brittle behavior of amorphous metals. J. Mech. Phys. Solids 31, 359–388.
Sun, L., Jiang, M.Q., Dai, L.H., 2010. Intrinsic correlation between dilatation and pressure sensitivity of plastic flow in metallic glasses. Scripta Mater. 63, 945–948.
Tong, W., Ravichandran, G., 1995. Inertial effects on void growth in porous viscoplastic materials. J. Appl. Mech. Trans. ASME 62, 633–639.
Tvergaard, V., Hutchinson, J.W., 1993. Effect of Initial void shape on the occurrence of cavitation instabilities in elastic-plastic solids. J. Appl. Mech. 60, 807–812.
Wu, X.Y., Ramesh, K.T., Wright, T.W., 2003. The coupled effects of plastic strain gradient and thermal softening on the dynamic growth of voids. Int. J. Solids Struct. 40, 6633–6651.